Article

SCIENCE PROGRESS

Science Progress
1–19

DOI: 10.1177/0036850419883565
journals.sagepub.com/home/sci
SAGE

Design of an active front steering system for a vehicle using an active disturbance rejection control method

Nan Sang and Lele Chen
School of Automotive Engineering, Changzhou Institute of Technology, Changzhou, China

Abstract

A linear vehicle model is commonly employed in the controller design for an active front steering (AFS). However, this simplified model has a considerable influence on the accuracy of the controller. In this article, an AFS controller using an active disturbance rejection control (ADRC) technique is proposed to prevent this problem. The AFS controller was established in MATLAB/Simulink to control the CarSim vehicle model for verification of the simulation. Under the straight-line driving disturbance condition, proportion-integration-differentiation (PID) control and ARDC substantially decreased with respect to the uncontrolled lateral offset and ADRC performed better than PID control. Under the double lane change (DLC) test working condition, the tracking error of the path, yaw rate, roll angle, and lateral acceleration, and error of the driving direction were used to evaluate the vehicle's controllability and stability. These evaluation indexes were substantially improved by PID control and ADRC; similarly, ADRC was better than PID control. The tracking error of the ADRC in the presence of parameter variance and external disturbance was significantly smaller than that of PID control. The results have verified that the AFS controller based on ADRC can significantly improve vehicle controllability and stability.

Keywords

active front steering, active disturbance rejection control, proportion-integration-differentiation control, controllability and stability, disturbance rejection

Introduction

Currently, driving safety has become the primary consideration in vehicle design and development, and the development of electronic techniques makes active

Corresponding author:
Nan Sang, School of Automotive Engineering, Changzhou Institute of Technology, 666 Liaohe Road, Xinbei District, Changzhou, Jiangsu Province 213032, China.
Email: sangn@czust.edu.cn

safety control possible. So in recent decades, various active safety control technologies have been applied to vehicles to improve their driving safety, from early anti-lock braking system, direct yaw-moment control (DYC), and electronic stability program to active steering system, collision-avoidance system (CAS), and so on. The application of these systems in vehicles has improved the longitudinal, yaw, and vertical dynamics of vehicles. Longitudinal dynamics control prevents wheel slip; lateral dynamics control prevents a yaw instability; and vertical dynamics control increases the ride comfort. Initially, longitudinal and yaw motions of a vehicle are controlled by changing the longitudinal force on a vehicle, which can improve longitudinal and yaw dynamics. However, the control of longitudinal and lateral motions is effective before the longitudinal force of tire saturation, and DYC controls the vehicle yaw motion by braking the wheel to change the wheel's longitudinal force to produce yaw moment. However, braking in normal driving will interfere with the driver's operation and affect ride comfort.[1] Active steering controls vehicle's longitudinal and lateral motion by changing the lateral force on a vehicle, which prevents these problems and fully utilizes the tire ground adhesion; it is one of the active safety systems that can directly contribute to the stability of a vehicle, especially regarding the controllability and stability.[2] This topic has gained attention in recent years and numerous control strategies for active steering have been proposed.[3–8]

Active front steering (AFS) is one type of active steering. AFS can be integrated with electric power steering and has been investigated and extensively applied to the yaw stability control of vehicle. Many researchers have deeply studied various yaw stability control methods based on AFS for the vehicle.[6–13] Zhao proposed a CAS for autonomous vehicle based on AFS, and designed an AFS robust tracking controller to improve path tracking performance in Wnag et al.[7] Zhao designed a H_∞ controller for AFS to ensure that the steering wheel torque accurately and quickly tracks the reference torque, and controllability, stability, and steering portability of a vehicle with AFS can be improved, as presented in Zhao et al.[8] The proportion-integration (PI),[6] proportion-integration-differentiation (PID), and fuzzy-PID control[9] methods were used for controller design of AFS to implement to track ideal yaw rate in the presence of model and parameter uncertainties and external perturbations to enhance yaw stability in emergencies. An AFS robust controller using a normalized left coprime factorization model is proposed in Ji et al.[10] As reported in Song,[11] considering the AFS system of BMW double planetary gear sets as the research object, Song proposed a sliding mode control method for AFS, which realizes the stability control of the vehicle in the tracking reference yaw rate. An AFS design method based on variable structure output feedback control is proposed to improve the stability of vehicles under under-steer and over-steer conditions in Ghoneim.[12] AFS based on quantitative feedback theory and with yaw rate as feedback parameter is discussed in Zhang et al.[13]

An additional front wheel angle input provided by AFS that is independent of a driver's action can improve vehicle's controllability and stability according to a vehicle's driving state in various conditions. Due to the additional angle, the

steering ratio is variable. By controlling the additional front wheel angle, AFS yields vehicle's actual steering characteristics that are similar to the ideal steering characteristics.

As previously mentioned, an AFS controller tracks the desired yaw rate to achieve yaw stability control. Following the active disturbance rejection control (ADRC) method is different from the previous method. The ADRC method can offer a linear, simple, and robust solution for some uncertain complex nonlinear systems.[14–16] In this article, the control of AFS is realized by the ADRC technique. The exogenous unknown disturbance (road roughness and crosswind) and endogenous unknown disturbance (tire nonlinearity, parameter variation, and load transfer) are considered as the disturbance of a vehicle. The PID algorithm,[17] optimal control algorithm,[18] and H_∞ robust control algorithm[19] are used to suppress the disturbance of a system. The PID algorithm has an excellent control effect on a linear system but the actual process is often nonlinear and time-varying. Due to the coupling and uncertainty of the parameters and structure, the application of classic PID method is difficult to get good control effect. The optimal control algorithm and H_∞ robust control algorithm depend on a highly precise model. The ADRC proposed by Prof. Han to suppress disturbances does not depend on a controlled system's accurate model. However, system disturbances are dynamically estimated according to tracking errors to realize the disturbance rejection and target tracking. In this article, disturbance suppression is realized, and the reference yaw rate is tracked by the ADRC technique.

The organization of article is as follows: the "AFS system" section introduces the AFS system, including steering model, tire model, and additional front wheel angle. The "Design of ADRC" section describes the design of AFS controller based on ADRC. In "Simulation experiments" section, some simulation results are provided to verify the effectiveness of different control strategies and to compare their control performance. In the "Conclusion" section, some conclusions are presented.

AFS system

Vehicle steering model

If disregarding the roll and pitch motion, the vehicle lateral motion (yaw rate ψ, and lateral acceleration a_y) can be described by a linear two-DOF (degrees of freedom) vehicle model. The single-track vehicle model is shown in Figure 1.

The equations of lateral and yaw motion for the single-track model will be derived as

$$\begin{cases} m(\dot{u}_y + u_x\psi) = F_{yf}\cos(\delta_f - \beta) + F_{yr}\cos\beta \\ I_z\dot{\psi} = F_{yf}l_f\cos\delta_f - F_{yr}l_r \end{cases} \quad (1)$$

where I_z is the moment of inertia for mass; m is the vehicle's mass; l_f and l_r are the distance from center of gravity to the front and rear wheel center, respectively; ψ is the yaw rate; β is the side-slip angle; δ_f is the front wheels angle; u_x and u_y is the

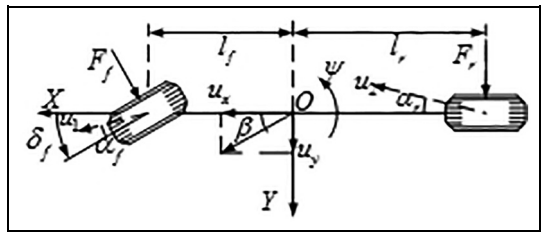

Figure 1. Single-track linear vehicle model.

longitudinal and lateral speed, respectively; F_{yf} and F_{yr} are the lateral force on the front and rear wheels, respectively.

Taking into account the constant longitudinal speed, small slip angles, and front wheel angles, and keeping the tire cornering stiffness linear are the basis of simplified vehicle model for a 2-DOF linear model. The cornering force that acts on the tires is related to the parameters $\alpha_{f,r}$ and $k_{1,2}$ as follows

$$\begin{cases} F_{yf} = k_1 \alpha_f \\ F_{yr} = k_2 \alpha_r \end{cases} \tag{2}$$

where k_1 and k_2 are the total cornering stiffness, and α_f and α_r are the sideslip angle.

As shown in Figure 1 and mentioned above, a small side-slip angle can be defined as

$$\beta = \arctan\left(\frac{u_y}{u_x}\right) \approx \frac{u_y}{u_x} \tag{3}$$

According to the regulation of the coordinate system in Figure 1, α_f and α_r are expressed by the following formulas

$$\begin{cases} \alpha_f = \beta + \dfrac{l_f \psi}{u_x} - \delta_f \\ \alpha_r = \beta + \dfrac{l_r \psi}{u_x} \end{cases} \tag{4}$$

Then, equation (1) can be rewritten as follows

$$\begin{cases} \dot{\psi} = \dfrac{l_f^2 k_1 + l_r^2 k_2}{I_z u_x} \psi + \dfrac{l_f k_1 - l_r k_2}{I_z} \beta - \dfrac{l_f k_1}{I_z} \delta_f \\ \dot{\beta} = \left(\dfrac{l_f k_1 - l_r k_2}{m u_x^2} - 1 \right) \psi + \dfrac{k_1 + k_2}{m u_x} \beta - \dfrac{k_1}{m u_x} \delta_f \end{cases} \tag{5}$$

Considering the derivative of both sides of equation (5) with respect to time t, and substituting $\beta = u_y/u_x$, $\dot{\beta} = \dot{u}_y/u_x$ and the lateral acceleration $a_y = \dot{u}_y + u_x\psi$ into equation (5), the following expressions can be derived

$$\begin{cases} \ddot{\psi} = \dfrac{l_f^2 k_1 + l_r^2 k_2}{I_z u_x}\dot{\psi} - \dfrac{l_f k_1 - l_r k_2}{I_z}\psi + \dfrac{l_f k_1 - l_r k_2}{I_z u_x}a_y - \dfrac{l_f k_1}{I_z}\dot{\delta}_f \\ \dot{a}_y = \dfrac{l_f k_1 - l_r k_2}{m u_x}\dot{\psi} - \dfrac{k_1 + k_2}{m}\psi + \dfrac{k_1 + k_2}{m}a_y - \dfrac{k_1}{m}\dot{\delta}_f \end{cases} \tag{6}$$

where a_y is the lateral acceleration.

δ_f is equal to δ_{sf} and δ_{af} if the steering system is an AFS system. δ_{sf} is the front wheel angle generated by the steering wheel angle; δ_{af} is the additional front wheel angle generated by an active steering system

$$\dot{\delta}_f = \dot{\delta}_{sf} + \dot{\delta}_{af} \tag{7}$$

Substituting $\dot{\delta}_f = \dot{\delta}_{sf} + \dot{\delta}_{af}$ into equation (6) yields

$$\ddot{\psi} = f_1\left(\psi, \dot{\psi}, a_y\right) + b_1\dot{\delta}_{sf} + b_1\dot{\delta}_{af} \tag{8a}$$

$$\dot{a}_y = f_2\left(\psi, \dot{\psi}, a_y\right) + b_2\dot{\delta}_{sf} + b_2\dot{\delta}_{af} \tag{8b}$$

where

$$f_1(\cdot) = \frac{l_f k_1 - l_r k_2}{I_z u_x}a_y + \frac{l_f^2 k_1 + l_r^2 k_2}{I_z u_x}\dot{\psi} - \frac{l_f k_1 - l_r k_2}{I_z}\psi$$

$$b_1 = -\frac{l_f k_1}{I_z}$$

$$f_2(\cdot) = \frac{k_1 + k_2}{m u_x}a_y + \frac{l_f k_1 - l_r k_2}{m u_x}\dot{\psi} - \frac{k_1 + k_2}{m}\psi$$

$$b_2 = -\frac{k_1}{m}$$

To simplify the linear model and facilitate the design of the controller, the tire cornering stiffness is usually taken as a fixed value, that is, the tire cornering characteristics are linearized. The cornering characteristics of a tire are nonlinear, and especially in the case of a vehicle in extreme working conditions or large lateral acceleration, the nonlinearity of tire cornering characteristics is distinct. The tire cornering stiffness is regarded as a fixed value for the controller design, and the system has parameter uncertainty, which has an impact on the control performance. A robust control design is usually required to eliminate this influence. Eliminating this disturbance in the controller design is easy if the disturbance caused by the parameter uncertainty can be accurately estimated. Since the ADRC technique can estimate and compensate the disturbance resulting from parameter uncertainty, it

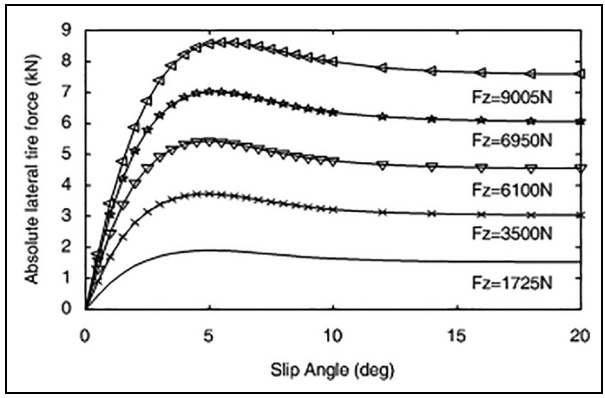

Figure 2. Lateral force characteristics of the tire.

has strong robustness to the parameter uncertainty, which is investigated in the following section. In this article, the tire side-slip characteristics is linear in the controller design. In the following series of simulation experiments, the lateral tire force data come from built-in tire model of CarSim software, which contains the nonlinear characteristics of the tire. The verification of the controller performance also includes partial verification of the controller's robustness to parameter uncertainty. The tire in the simulation vehicle is 185/65 R15 and its lateral force characteristics are shown in Figure 2 (data from CarSim software). In Figure 2, F_z is the vertical force of the tire.

Additional steering angle of front road wheel

AFS is implemented by motion superposition such as BMW's, its structure is shown in Figure 3. The input end of the 2-DOF planetary gear set is the steering wheel, and its output end is connected to the rack and pinion steering gear. δ_p is the input angle of the steering gear, where the rotated direction of δ_p is consistent with the steering wheel input θ_{sw}, where $\theta_{sw} = G \cdot \delta_{sf}$ (G is ratio of the steering gear), and δ_p was obtained by the superposition of θ_{sw} and θ_{ac}, and θ_{ac} is the angle of the active steering motor.

Design of ADRC

Control structure of AFS

By controlling the additional front wheel angle, the AFS controlled by ADRC enables the vehicle to track the ideal yaw rate; the control diagram is shown in Figure 4.

ADRC employs a feedback controller, whose control inputs are ψ and ψ_d, and the control output is θ_{FB}. The relationship between θ_{FB} and θ_{ac} is decided by the

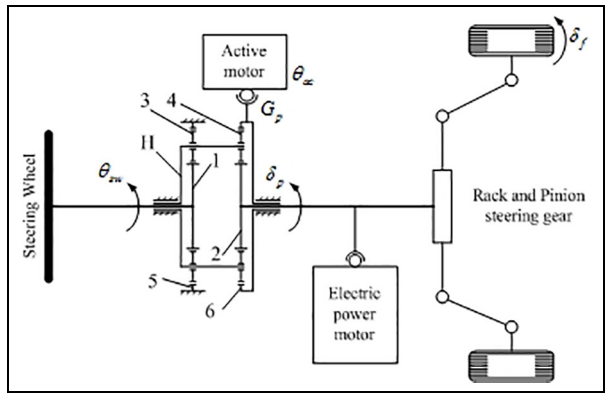

Figure 3. A schematic diagram of active front wheel steering system.
1, 2: sun gear; 3, 4: planetary gear; 5: fixed gear ring; 6: gear ring; H: planetary gear carrier.

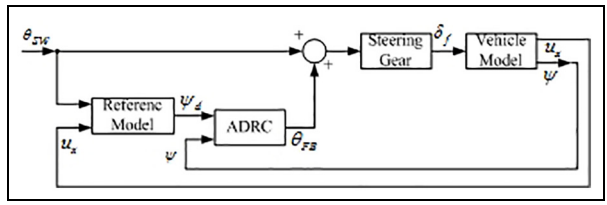

Figure 4. Control structure of AFS.

structure and parameters of the planetary gear set. As shown in Figure 3, this relationship is $\theta_{FB} = -\theta_{ac} \cdot z_6/z_1/G_p$ (G_p is the reduction ratio, and z_1 and z_6 are the teeth of the corresponding gear).

Let $\psi_r = \theta_{sw} \cdot u_x/L/(1 + Ku_x^2)/G$. Considering the road adhesion coefficient, the reference yaw rate ψ_d is expressed as

$$\psi_d = \begin{cases} \psi_r, & |\psi_r| \le \mu \dfrac{g}{u_x} \\ \mathbf{sign}(\psi_r)\mu \dfrac{g}{u_x}, & \text{other} \end{cases} \tag{9}$$

where **sign** is the signum function; μ is the road adhesion coefficient; $L = l_f + l_r$; K is the understeer coefficient; and g is the acceleration of gravity.

Design of ADRC for AFS

The ADRC technique and the design of ADRC is proposed and discussed by Han.[20] The design process of ADRC for AFS is described as follows:

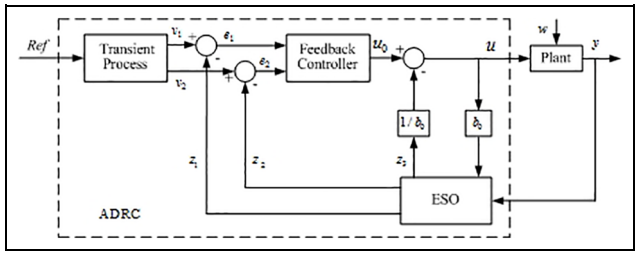

Figure 5. Control structure of the second-order ADRC.

In the ADRC technique, the exogenous unknown disturbance, endogenous unknown disturbance, and so on are considered as the total disturbance. If the input and output of the system can be measured, the total disturbance can be dynamically estimated using extended state observer (ESO) without knowing the disturbance model, and the suppressing disturbance and tracking target are implemented by the feedback compensation.

Set $\dot{x}_1 = x_2 = \dot{\psi}$; equation (8a) can be written as the following two-order system

$$\begin{cases} \dot{x}_1 = x_2 \\ \dot{x}_2 = f_1(\psi, \dot{\psi}, a_y) + B_1\dot{\theta}_{sw} + B_1\dot{\theta}_{FB} \\ y^* = x_1 \end{cases} \tag{10}$$

where $B_1 = b_1/G$; and $\dot{\theta}_{sw}$ is the differential of θ_{sw} and can be obtained by the tracking-differentiator (TD) function (FTD)[21]

$$\begin{cases} f_{td} = \boldsymbol{FTD}(\zeta_1 - \theta_{sw}, \zeta_2, r, h) \\ \dot{\zeta}_1 = \zeta_2, \dot{\zeta}_2 = f_{td} \end{cases} \tag{11}$$

where ζ_1 and ζ_2 estimate the approximated value of θ_{sw} and $\dot{\theta}_{sw}$, respectively. The $\boldsymbol{FTD}(\cdot)$ can be obtained from Han,[20] its expression is

$$\begin{cases} c = rh^2, d_0 = hy_2, y = y_1 + d_0 \\ d_1 = \sqrt{c(c + 8|y|)}, d_2 = d_0 + \mathbf{sign}(y)\dfrac{(d_1 - c)}{2} \\ d = (d_0 + y)\boldsymbol{fbg}(y, c) + d_2(1 - \boldsymbol{fbg}(y, c)) \\ \boldsymbol{FTD}(y_1, y_2, r, h) = -r\left(\dfrac{d}{c}\right)\boldsymbol{fbg}(d, c) - r\mathbf{sign}(d)(1 - \boldsymbol{fbg}(d, c)) \end{cases} \tag{12}$$

where $\boldsymbol{fbg}(d, c) = (\mathbf{sign}(d + c) - \mathbf{sign}(d - c))/2$; h is the integral step; and r is the tracking speed factor.

The desired reference yaw rate can be tracked by the second-order ADRC as shown in equation (8a). The general structure of the second-order ADRC is shown in Figure 5. The design of ADRC generally includes the following steps.

Transient process. The transient process has an important role in the ADRC according to the research results by Huang.[20] The transient process of the tracking target can solve the contradiction between overshoot and quick-response ability and increase the adjustable scope of the controller parameters, which enhances the controller robustness. The transient process of the tracking target can be realized by the $\boldsymbol{FTD}(\cdot)$.[21]

$$\begin{cases} f_{td} = \boldsymbol{FTD}\left(\zeta_1^* - \psi_d, \zeta_2^*, r, h\right) \\ \dot{\zeta}_1^* = \zeta_2^*, \dot{\zeta}_2^* = f_{td} \end{cases} \tag{13}$$

Equation (13) realizes the transient process of the tracking signal ψ_d. Its differential signal ζ_2^* can be achieved and applied in the state error feedback of ADRC.

ESO. If the total disturbance $f_1(\cdot)$ can be extended to the system state x_3, equation (10) can be extended to the third-order ESO, which can estimate the system states x_1 and x_2 and the total disturbance $f_1(\cdot)$. The total disturbance $f_1(\cdot)$ includes the system nonlinearity and model uncertainties, the road disturbance, and the crosswind. The third-order ESO algorithm can be expressed as

$$\begin{cases} \Theta = \upsilon_1 - y^* \\ \dot{\upsilon}_1 = \upsilon_2 - \beta_1 \cdot \Theta \\ \dot{\upsilon}_2 = \upsilon_3 - \beta_2 \cdot \boldsymbol{F}_{non}(\Theta, \xi, \Delta) + B_1 \dot{\theta}_{\mathrm{SW}} + B_1 \dot{\theta}_{\mathrm{FB}} \\ \dot{\upsilon}_3 = -\beta_3 \cdot \boldsymbol{F}_{non}(\Theta, \xi_1, \Delta_1) \end{cases} \tag{14}$$

where Θ is the error of x_1 and its estimated value, and β_1, β_2, and β_3 are the ESO gains. If the real value of B_1 is unknown, B_1 may be the approximated value from equation (14), which is empirically chosen but does not affect the control accuracy of ADRC. Then, the scheme of implementing feedback control and interference suppression using approximate variables is shown in Figure 4.

Equation (14) is the third-order ESO after equation (10) for the extended state. Compared with typical nonlinear state observers, the ESO can dynamically estimate the total disturbance of a system in real time. If β_1, β_2, and β_3 and the nonlinear function $\boldsymbol{F}_{non}(\Theta, \xi, \Delta)$ are selected suitably, the third-order ESO can implement the following process: υ_1 estimates the value of x_1, υ_2 estimates the value of x_2, and υ_3 estimates the value of x_3, where $x_3 = f_1(\psi, \dot{\psi}, a_y)$. The nonlinear function $\boldsymbol{F}_{non}(\cdot)$ can exhibit different forms. In this article, $\boldsymbol{F}_{non}(\cdot)$ can be expressed as

$$\boldsymbol{F}_{non}(\Theta, \xi, \Delta) = \begin{cases} |\Theta|^{\xi} \mathbf{sign}(\Theta), & |\Theta| > \Delta \\ \Theta \Delta^{\xi - 1}, & |\Theta| \le \Delta \end{cases} \tag{15}$$

where ξ and Δ are positive numbers.

Feedback control law. An ADRC feedback control law consists of state errors. The state errors of the system—$\Theta_1 = \zeta_1^* - \upsilon_1$ and $\Theta_2 = \zeta_2^* - \upsilon_2$—generate the nonlinear or linear feedback control law u_0, and is expressed as

$$u_0 = \beta_{01}\Theta_1 + \beta_{02}\Theta_2 \tag{16}$$

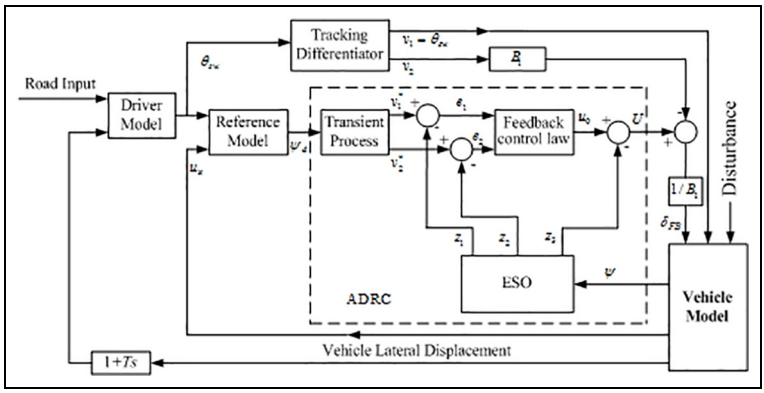

Figure 6. The closed-loop control structure of AFS system.

The error feedback control law of equation (16) includes the yaw rate error and its differential signal. More system state information is employed, which improves the control effect.

Final feedback control law. Setting $B_1\dot{\theta}_{sw} + B_1\dot{\theta}_{FB} = u_0 - \upsilon_3$, the final feedback control law u can be dynamically obtained by the ESO using u_0 and υ_3

$$u = \dot{\theta}_{FB} = \frac{\left(u_0 - \upsilon_3 - B_1\dot{\theta}_{sw}\right)}{B_1} \tag{17}$$

Therefore, the υ_3/B_1 compensates the total disturbances of the system. The closed-loop steering control structure of the vehicle with AFS is shown in Figure 6, where the reference model is the linear vehicle model, the driver model is the single point preview driver model, and T is the driver preview time.

Stability analysis of ADRC

The system of equations (10) was controlled by ADRC, including the ESO of equation (14) and the control law of equation (17). Wan[22] suggested that the necessary condition for absolute stability of the system is $\mathrm{Re}\lambda(A)>0$ and the controller parameters $\beta_i>0$. Matrix **A** consists of the coefficients of equations (10), (14), and (17). The detailed derivation is provided in Wan[22]

$$\boldsymbol{A} = \begin{bmatrix} A_{11} & A_{11}A_{12} \\ 0 & A_{22} \end{bmatrix} \tag{18}$$

where $A_{11} = \begin{bmatrix} 0 & 1 \\ -a_2 & -a_1 \end{bmatrix}$, $A_{12} = \begin{bmatrix} 0 & 0 \\ -B_1\beta_{01} & -B_1\beta_{02} \end{bmatrix}$, $A_{12} = \begin{bmatrix} 0 & 1 \\ -B_1\beta_{01} & -B_1\beta_{02} \end{bmatrix}$, $a_1 = -(l_f^2k_1 + l_r^2k_2)/I_zu_x$, $a_2 = (l_fk_1 - l_rk_2)/I_z$.

Table 1. The main parameters of the vehicle.

Parameter	Value
Total mass of vehicle, m (kg)	1250
Distance from front axle to center of gravity, l_f (m)	1.25
Distance from rear axle to center of gravity, l_r (m)	1.55
Moment of inertia about the z-axis, I_z (kg m^2)	2400
Steering gear ratio, G	20

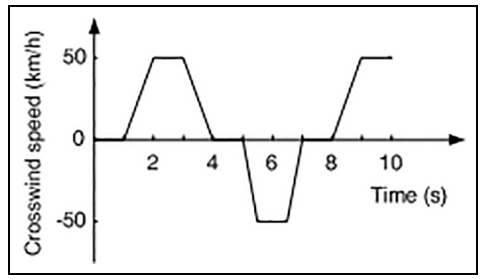

Figure 7. Random crosswind.

For the convergence of the ADRC controller, ESO, and TD, Zhao has constructed a mathematical proof in his doctoral dissertation.[23]

Simulation experiments

To verify the control performance of ADRC in active front wheel steering, MATLAB software was used to control the CarSim vehicle model for the test with straight-line driving and double lane change (DLC) test conditions. The test results in three cases (no control, PID control, and ADRC) are compared. The simulating parameters of ADRC are $\beta_1 = 100$, $\beta_2 = 200$, and $\beta_3 = 300$; the PID controller parameters are $K_p = 10$, $K_i = 100$, and $K_d = 0.5$. The tire and suspension model of the simulated vehicle was built by CarSim software. The main parameters of the simulated vehicle are shown in Table 1.

Disturbance rejection test for straight-line driving

Working conditions: The vehicles have no steering wheel input, road surface (roughness coefficient $G_0 = 5\times10^{-6}$) disturbance, and random crosswind disturbance (as shown in Figure 7), and the vehicle direction is perpendicular to the velocity of the vehicle. The road adhesion coefficient $\mu = 0.8$; the vehicle speed $u_x = 80$ km/h; and the vehicle operates with straight-line driving.

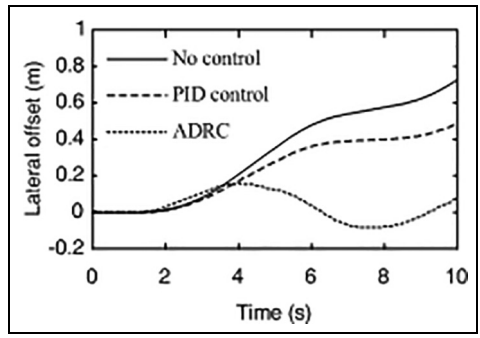

Figure 8. Disturbance rejection test for straight-line driving.

Figure 8 shows the results of the disturbance rejection test of straight-line driving. Due to the road roughness disturbance and crosswind disturbance, the vehicle without a controller and the vehicle with a PID controller deviate from the straight path. At the end of the test, the maximum lateral deviation for uncontrolled vehicle is 0.73 m, the maximum lateral deviation for PID-controlled vehicle is 0.49 m, and their driving paths are biased to the left of the vehicle. The maximum lateral deviation for ADRC vehicle during the entire test is 0.14 m, and its driving path is on either side of the desired vehicle path. ADRC has excellent disturbance rejection ability and is superior to PID controller.

DLC test evaluation (u_x = 100 km/h)

The speed of the standard DLC test is $u_x = 80$ km/h. The purpose of the $u_x = 100$ km/h high-speed DLC test is to verify the controller performance in extreme conditions. In the high-speed DLC test, the road roughness coefficient is $G_0 = 5\times10^{-6}$; the test path and the position of the cone are set up according to the standard test for adaptive setting with speed change, as shown in Figure 9.

Figure 10 shows the results of DLC test for three cases (no control, PID control, and ADRC), where Figure 10(a)–(f) shows the vehicle trajectory, yaw rate, side-slip angle, lateral acceleration, roll angle, and active steering control input (front wheels), respectively.

Figure 10(a) shows the vehicle path tracking of the DLC test. The results using the PID controller and ADRC are significantly better than the results without a controller. The uncontrolled vehicle trajectory has a large deviation from the expected path in the S3, S4, and S5 sections. In the straight-line segment (S5 and S6), the lateral displacement overshoot of the uncontrolled vehicle is 0.40 m, which is significantly larger than that of 0.17 m for the PID-controlled vehicle and that of 0.1 m for the ADRC vehicle. Both PID control and ADRC can effectively suppress the lateral displacement overshoot and obtain better path tracking response characteristics, among which ADRC is slightly better than PID control. Both the

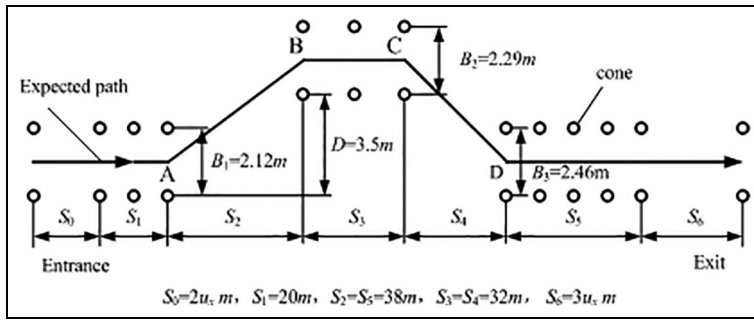

Figure 9. The test path and the position of the cone in double lane change test.

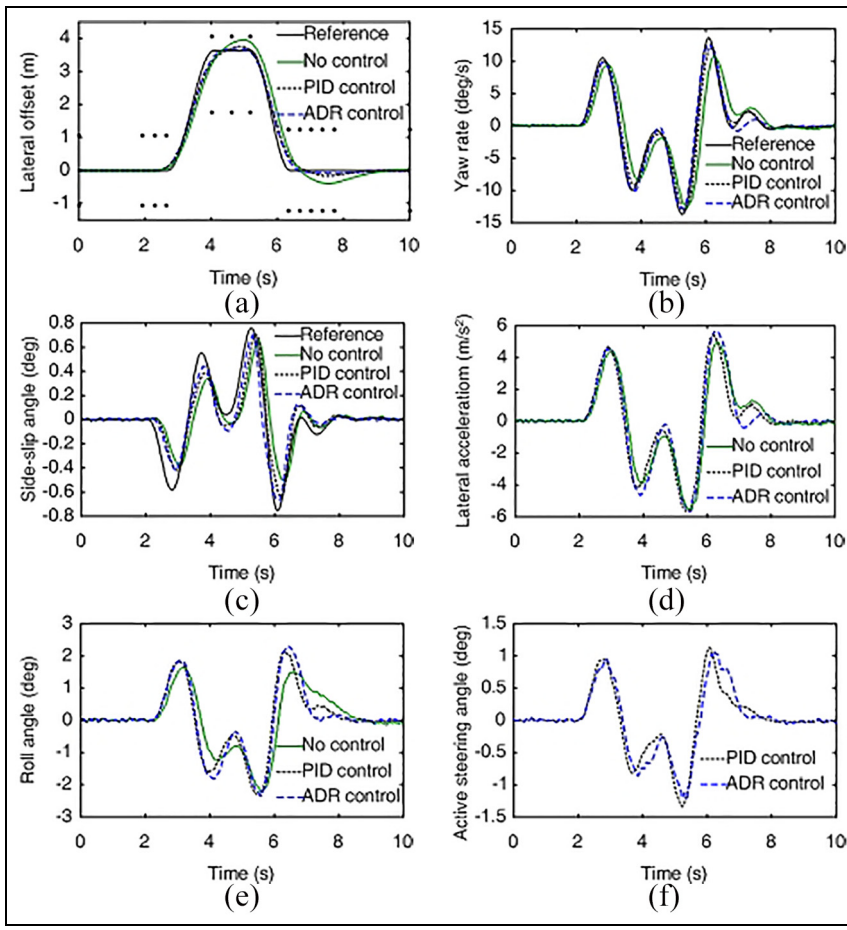

Figure 10. Double lane change test: (a) vehicle trajectory, (b) yaw rate, (c) side-slip angle, (d) lateral acceleration, (e) roll angle, and (f) active steering angle.

PID-controlled vehicle and the ADRC vehicle can well complete the DLC test, while the uncontrolled vehicle cannot complete the DLC test. The collision cone phenomenon occurs in the test process.

Figure 10(b) and (c) is the tracking properties of the ideal yaw rate and side-slip angle for uncontrolled vehicle and controlled vehicle, respectively. The tracking errors of the yaw rate and side-slip angles of the controlled vehicle are substantially smaller than those of the uncontrolled, and the response hysteretic time of the uncontrolled vehicle is greater than that of the controlled. The tracking performance of ADRC for the target value is better than that of PID control.

From Figure 10(d) and (e), we determine that the roll angles and lateral acceleration of the PID-controlled and ADRC vehicles are larger than those of the uncontrolled vehicle. To ensure the steering stability of vehicles, all commercial vehicles in use have understeering characteristics. To track the ideal yaw rate, the steering wheel should turn at a greater angle and generate a greater lateral acceleration. If no roll control exists, the change trend of the roll angle is consistent with the lateral acceleration.

The DLC test results qualitatively show that the AFS vehicle controlled by ADRC has a strong path tracking capability.

In this article, the path tracking error index, driving direction error index, lateral acceleration evaluation index, roll angle evaluation index, and yaw rate tracking error index are quantitatively evaluated for the closed-loop controllability and stability. The evaluation indexes are defined as follows:

- The path tracking error index J_{e1}

$$J_{e1} = \int_0^{t_n} [f(\tau) - y(\tau)]^2 d\tau \tag{19}$$

where t_n is the duration of the test; $f(\tau)$ is the desired path; and $y(\tau)$ is the actual driving path of the vehicle.

- The driving direction error index J_{e2}

$$J_{e2} = \int_0^{t_n} [u_x(\tau)\beta(\tau)]^2 d\tau \tag{20}$$

- The lateral acceleration evaluation index J_{r1}

$$J_{r1} = \int_0^{t_n} [a_y(\tau)]^2 d\tau \tag{21}$$

- The roll angle evaluation index J_{r2}

Table 2. Evaluation index result of double lane change test at u_x = 100 km/h.

Control state / Index	No control	PID control		ADRC control	
	Value	Value	Decrease(%)	Value	Decrease(%)
J_{e1}	8.9183	1.3806	–84.50%	0.4204	–95.30%
J_{e2}	0.0213	0.0206	–3.29%	0.0193	–9.39%
J_{r1}	5.3160	5.0970	–4.11%	4.7260	–11.10%
J_{r2}	0.2330	0.2250	–3.43%	0.1870	–19.70%
J_R	0.3197	0. 2563	–19.80%	0.1933	–39.50%

PID: proportion-integration-differentiation. ADRC: active disturbance rejection control.

$$J_{r2} = \int_0^{t_n} [\varphi(\tau)]^2 d\tau \tag{22}$$

where $\varphi(\tau)$ is the vehicle actual roll angle.

- The yaw rate tracking error index J_R

$$J_R = \int_0^{t_n} [\psi_d(\tau) - \psi(\tau)]^2 d\tau \tag{23}$$

The manipulation stability evaluation indexes of the DLC test are quantitatively calculated according to equations (19)–(23), as shown in Table 2. The descent rate of each evaluation index of the PID-controlled and ADRC vehicles relative to that of the uncontrolled vehicle are provided.

For the closed-loop control test evaluation indicators J_{e1}, J_{e1}, J_{r1}, J_{r2}, and J_R, the PID-controlled vehicle decreased by 84.5%, 3.29%, 4.11%, 3.43%, and 19.8%, respectively, and the ADRC vehicle decreased by 95.3%, 9.39%, 11.1%, 19.7%, and 39.5%, respectively, compared with the uncontrolled. The evaluation indicators of the PID-controlled and ADRC vehicles exhibit a significant decrease, and the controllability and stability of the vehicle are improved, especially the index that employs ADRC control. Among these indicators, the improvement in J_{e1} and J_R is the most distinct, which indicates that the controller has better tracking performance, which is consistent with the qualitative analysis results.

Robust analysis of controllers on sprung mass variation (u_x = 100 km/h)

The most important function of the vehicle is to carry passengers or transport goods. The sprung mass of the vehicle will vary in different occasions. For example, the load variation, load distribution variation, and load transfer in turning will cause vertical load variations of the tire and variation in the tire cornering

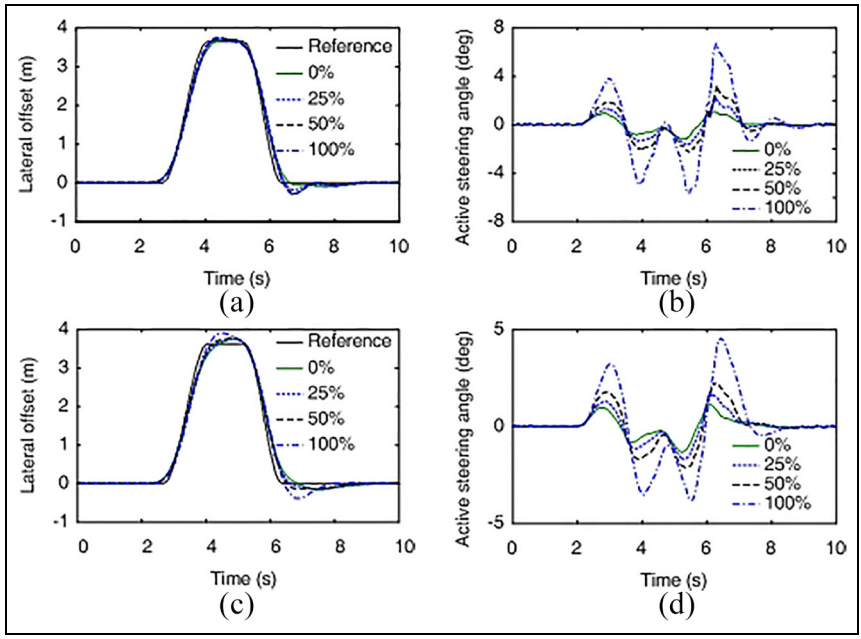

Figure 11. Impact of sprung mass variation on controller performance: (a) vehicle trajectory (ADRC), (b) active steering angle (ADRC), (c) vehicle trajectory (PID), and (d) active steering angle (PID).

characteristics, which affect the controllability and stability. The following tests were used to verify the robustness of ADRC and PID controller in the presence of the variations in the vehicle sprung mass. In the test, the added mass is assumed to be loaded on the suspension; the increased mass percentages are 0%, 25%, 50%, and 100%; and the other parameters of the vehicle and the controller parameters are not changed. Figure 11 shows the test results. Figure 11(a) and (b) shows the path tracking result and the active input of the front wheel of the vehicle with ADRC, respectively, and Figure 11(c) and (d) is the path tracking result and the active input of the front wheel of the vehicle with PID control, respectively. With the increase of the sprung mass, the active inputs of the front wheel using ADRC and PID control increase, the driving path concentration of the vehicle with ADRC is better than that of PID control, and its deviation from the expected path is smaller than the PID-controlled vehicle. The test results show that ADRC is more robust to variations of the vehicle sprung mass than the PID controller.

As previously mentioned, the tires in the CarSim vehicle model have nonlinear characteristics, and its parameters are variable during the working process. In this section, the controller to the robustness of sprung mass uncertainty is verified. Although the other parameters of the test vehicle used by the controller are also fixed values, these parameters, such as suspension parameters, the position of the

vehicle mass center, and the moment of inertia, are variable, and modeling errors exist. These results show that ADRC has excellent robustness.

Conclusion

The AFS controller using ADRC technique is proposed to realize the active steering control for a vehicle, follow the ideal yaw rate, and ensure that the vehicle is working within the safety threshold. At the same time, the vehicle with AFS has better controllability and stability. The results show that ADRC controller has better path tracking ability and stronger robustness to the vehicle mass variation than the PID controller. The design procedure of ADRC also indicates that it does not require a high-accuracy model and is not specific to the problem, which has excellent portability. Because ADRC can estimate various disturbances in real time and dynamically compensate them during the working process, it has an excellent control effect on the nonlinear system. The proposed AFS control method based on the ADRC technique provides a new method to deal with nonlinear problems, disturbance suppression, and coupling control.

ADRC technology is developed based on the practical application and lacks in-depth theoretical research. Parameters tuning is also based on personal experience. Future research will focus on these two aspects.

Declaration of conflicting interests

The author(s) declared no potential conflicts of interest with respect to the research, authorship, and/or publication of this article.

Funding

The author(s) disclosed receipt of the following financial support for the research, authorship, and/or publication of this article: This work was supported by National Natural Science Foundation of China under Grant No. 51775268 and Natural Science Foundation of the Jiangsu Higher Education Institutions of China under Grant No. 18KJB590001.

ORCID iD

Nan Sang https://orcid.org/0000-0002-5735-2301

References

1. He J, Crolla DA, Levesley MC, et al. Coordination of active steering, driveline, and braking for integrated vehicle dynamics control. *Proc IMechE, Part D: J Automobile Engineering* 2006; 220(10): 1401–1421.
2. Truong DVT and Tomaske W. Active front steering system using adaptive sliding mode control. In: *2013 25th Chinese control and decision conference (CCDC)*, Guiyang, China, 25–27 May 2013, pp. 253–258. New York: IEEE.

3. Mammar S and Koenig D. Vehicle handling improvement by active steering. *Vehicle Syst Dyn* 2002; 38(3): 211–242.
4. Hiraoka T, Nishihara O and Kumamoto H. Model-following sliding mode control for active four-wheel steering vehicle. *JSAE Rev* 2004; 25(3): 305–313.
5. Akar M. Yaw rate and sideslip tracking for 4-wheel steering cars using sliding mode control. In: *2006 IEEE international symposium on computer aided control system design*, Munich, 4–6 October 2006, pp. 1300–1305. New York: IEEE.
6. Yu N. Yaw control enhancement for buses by active front steering. PhD Dissertation, The Pennsylvania State University, State College, PA, 2007.
7. Wnag CY, Zhao WZ, Xu ZJ, et al. Path planning and stability control of collision avoidance system based on active front steering. *Sci China Technol Sci* 2017; 60(8): 1231–1243.
8. Zhao WZ, Li YJ and Wang CY. Robust control of hand wheel torque for active front steering system. *Sci China Technol Sci* 2015; 58(1): 107–116.
9. Dan X, Chi Y, Huang K, et al. Controlling strategy research on active front steering system. In: *2011 international conference on consumer electronics, communications and networks (CECNet)*, Xianning, China, 16–18 April 2011, pp. 4871–4874. New York: IEEE.
10. Ji X, Wu J, Zhao Y, et al. A new robust control method for active front steering considering the intention of the driver. *Proc IMechE, Part D: J Automobile Engineering* 2015; 229(4): 518–531.
11. Song J. Active front wheel steering model and controller for integrated dynamics control systems. *Int J Auto Techn* 2016; 17(2): 265–272.
12. Ghoneim YA. Application of variable-structure output feedback control to active front steering for understeer and oversteer conditions. *Int J Vehicle Des* 2013; 62(2–4): 106–122.
13. Zhang JY, Kim JW, Lee KB, et al. Development of an active front steering (AFS) system with QFT control. *Int J Auto Techn* 2008; 9(6): 695–702.
14. Han J. From PID technique to active disturbances rejection control technique. *Control Eng China* 2002; 9(3): 13–18 (in Chinese).
15. Chen Z-Q, Zhao J-X and Yuan Z-Z. An active disturbances rejection controller for hysteretic systems. *Int J Model Ident Contr* 2009; 7(1): 113–118.
16. Zhu H-Q, Chen J-J and Sun X-D. Active disturbances rejection decoupling control for active magnetic bearing multivariable system. *Int J Model Ident Contr* 2009; 7(1): 119–125.
17. Hasbullah F, Faris WF, Darsivan FJ, et al. Ride comfort performance of a vehicle using active suspension system with active disturbance rejection control. *Int J Vehicle Noise Vib* 2015; 11(1): 78–101.
18. Yang X, Wang Z and Peng W. Coordinated control of AFS and DYC for vehicle handling and stability based on optimal guaranteed cost theory. *Vehicle Syst Dyn* 2009; 47(1): 57–79.
19. Li J and Zhang J. H∞ robust control for integrated chassis system based on state feedback. *J Jilin Univ (Eng Technol Edition)* 2016; 46(3): 57–79 (in Chinese).
20. Han J. *Active disturbance rejection control technique: the technique for estimating and compensating the uncertainties*. Beijing, China: National Defense Industry Press, 2008 (in Chinese).
21. Huang H, Wan H and Han J. Arranging the transient process is an effective method improved the "robustness, adaptability and stability" of closed-loop system. *Contr Theory Appl* 2001; 18(Suppl.): 89–94.

22. Wan H. Absolute stability analysis of active disturbance rejection controller. *J Shanghai Univ Electr Power* 2011; 27(5): 507–511.
23. Zhao Z. Convergence of nonlinear active disturbance rejection control. *Doctoral Dissertation, University of Science and Technology of China, Hefei, China*, 2012.

Author biographies

Nan Sang received his BEng in Vehicle Engineering from Wuhan Institute of Technology in 1991, his MEng in Vehicle Engineering from Wuhan University of Technology in 2003, and a PhD degree from the Department of Vehicle Engineering, Nanjing University of Aeronautics and Astronautics, China, in 2018. Currently, he is a Professor in the Department of Automobile Engineering, Changzhou Institute of Technology. His research interests include vehicle dynamics and control.

Lele Chen received her MS degree in Applied Mathematics from Jiangsu University in 2010 and her PhD degree in Fluid Dynamics from Nanjing University of Aeronautics and Astronautics in 2017. Currently, she is a lecturer in School of Automotive Engineering, Changzhou Institute of Technology, China, and her research interests include computational aerodynamics.